

PAPER

Chirp- and random-based coded ultrasonic excitation for localized blood-brain barrier opening

To cite this article: H A S Kamimura *et al* 2015 *Phys. Med. Biol.* **60** 7695

View the [article online](#) for updates and enhancements.

Related content

- [Acoustic cavitation-based monitoring of the reversibility and permeability of ultrasound-induced blood-brain barrier opening](#)
Tao Sun, Gesthimani Samiotaki, Shutao Wang *et al.*
- [In vivo transcranial cavitation detection during ultrasound-induced BBB opening](#)
Yao-Sheng Tung, Fotios Vlachos, James J Choi *et al.*
- [Permeability assessment of the FUS-induced BBB opening using dynamic contrast-enhanced MRI](#)
F Vlachos, Y-S Tung and E E Konofagou

Recent citations

- [Amelioration of the nigrostriatal pathway facilitated by ultrasound-mediated neurotrophic delivery in early Parkinson's disease](#)
Maria Eleni Karakatsani *et al*
- [Enhanced Numerical Method for the Design of 3-D-Printed Holographic Acoustic Lenses for Aberration Correction of Single-Element Transcranial Focused Ultrasound](#)
Marcelino Ferri *et al*
- [Acoustically targeted chemogenetics for the non-invasive control of neural circuits](#)
Jerzy O. Szablowski *et al*

varian | RapidPlan & MCO

Machine learning powered by (you)

Take knowledge-based planning to an intelligent new level.

Power new victories >

Chirp- and random-based coded ultrasonic excitation for localized blood-brain barrier opening

H A S Kamimura^{1, 2}, S Wang¹, S-Y Wu¹, M E Karakatsani¹,
C Acosta¹, A A O Carneiro² and E E Konofagou¹

¹ Department of Biomedical Engineering, Columbia University, New York, NY, USA

² Department of Physics, Faculdade de Filosofia, Ciências e Letras de Ribeirão Preto, Universidade de São Paulo, Ribeirão Preto, SP, Brazil

E-mail: ek2191@columbia.edu

Received 2 June 2015, revised 11 August 2015

Accepted for publication 27 August 2015

Published 22 September 2015



Abstract

Chirp- and random-based coded excitation methods have been proposed to reduce standing wave formation and improve focusing of transcranial ultrasound. However, no clear evidence has been shown to support the benefits of these ultrasonic excitation sequences *in vivo*. This study evaluates the chirp and periodic selection of random frequency (PSRF) coded-excitation methods for opening the blood-brain barrier (BBB) in mice. Three groups of mice ($n = 15$) were injected with polydisperse microbubbles and sonicated in the caudate putamen using the chirp/PSRF coded (bandwidth: 1.5–1.9 MHz, peak negative pressure: 0.52 MPa, duration: 30 s) or standard ultrasound (frequency: 1.5 MHz, pressure: 0.52 MPa, burst duration: 20 ms, duration: 5 min) sequences. T1-weighted contrast-enhanced MRI scans were performed to quantitatively analyze focused ultrasound induced BBB opening. The mean opening volumes evaluated from the MRI were $9.38 \pm 5.71 \text{ mm}^3$, $8.91 \pm 3.91 \text{ mm}^3$ and $35.47 \pm 5.10 \text{ mm}^3$ for the chirp, random and regular sonications, respectively. The mean cavitation levels were $55.40 \pm 28.43 \text{ V.s}$, $63.87 \pm 29.97 \text{ V.s}$ and $356.52 \pm 257.15 \text{ V.s}$ for the chirp, random and regular sonications, respectively. The chirp and PSRF coded pulsing sequences improved the BBB opening localization by inducing lower cavitation levels and smaller opening volumes compared to results of the regular sonication technique. Larger bandwidths were associated with more focused targeting but were limited by the frequency response of the transducer, the skull attenuation and the microbubbles optimal frequency range. The coded methods could therefore facilitate highly localized drug delivery as well as benefit other transcranial ultrasound techniques that use higher pressure levels and higher precision to

induce the necessary bioeffects in a brain region while avoiding damage to the surrounding healthy tissue.

Keywords: blood-brain barrier opening, chirp, coded ultrasonic excitation, focused ultrasound, standing wave, transcranial ultrasound

(Some figures may appear in colour only in the online journal)

1. Introduction

The potential of noninvasive focused ultrasound (FUS) for enhancing drug delivery or as a substitute for surgical intervention has been demonstrated for the treatment of a variety of neurological disorders. In the first case, the administration of FUS combined with microbubbles has been shown to transiently and locally open the blood-brain barrier (BBB) (Hynynen *et al* 2001, Choi *et al* 2007) allowing the passage of pharmacological agents such as anticancer therapeutic drugs (Kinoshita *et al* 2006), therapeutic antibodies (Raymond *et al* 2008), neurotrophic factors (Baseri *et al* 2012), adeno-associated virus (Alonso *et al* 2013, Wang *et al* 2015), and neural stem cells (Burgess *et al* 2011). Ultrasound has also been proven capable of enhancing the fibrinolytic effect of drugs used in ischemic stroke for dissolving blood clots—known as sonothrombolysis (Alexandrov 2009, Meairs *et al* 2012). Furthermore, the High-Intensity Focused Ultrasound (HIFU) can thermally annihilate brain tumors (Coluccia *et al* 2014) or brain tissue cells. Brain ablation can reduce hyper-excitability activity of neurons in such cases as essential tremors (Chang *et al* 2015, Elias *et al* 2013) and chronic neuropathic pain (Martin *et al* 2009). More recently, ultrasound has also been proven capable of modulating the neuronal activity (Tyler *et al* 2008, Deffieux *et al* 2013, King *et al* 2013) providing thus a wider range of applications of FUS as an alternative for the transcranial magnetic stimulation, deep brain stimulation, and optogenetics.

The use of ultrasound for the treatment of neurological disorders remains challenging because of the skull. The high attenuation coefficient, variable thickness and heterogeneity of the skull cause scattering and absorption of ultrasound waves. As a result, the ultrasound beam can be distorted due to aberration effects and standing waves that can be formed, which in turn prevent correct targeting through the skull. Incorrect targeting when using high power ultrasound (sonothrombolysis, tumor ablation) may lead to severe adverse effects such as hemorrhage and the permanent damage of healthy tissues (Daffertshofer *et al* 2005, Molina *et al* 2009, Tsiygoulis *et al* 2010). Moreover, the use of microbubbles aggravates the adverse effects provoked by cavitation.

Several approaches were proposed and examined in order to achieve an effective transcranial sonication. Large phased arrays have been used for the correction of ultrasound focusing with computed tomographic based corrections of the phase and amplitude ultrasound signals (Hynynen and Jolesz 1998, Hynynen *et al* 2006, Marquet *et al* 2013, Pajek and Hynynen 2013). The chirp-coded ultrasonic excitation method has been used in the diagnostic ultrasound as a technique to improve range, resolution, signal-to-noise ratio of images (O'Donnell 1992, Pedersen *et al* 2003, Cobbold 2007) and it has been demonstrated capable of reducing standing waves for both diagnostic (Mitri *et al* 2005) and therapeutic ultrasound (Deffieux and Konofagou 2010). In addition, standing wave formation can be minimized using other methods such as multiple ultrasonic beams (Kamimura *et al* 2013), short pulses coded ultrasonic excitation (Choi *et al* 2011, O'Reilly *et al* 2011), and random-based coded ultrasonic excitation (Tang and Clement 2010, Furuhashi and Saito 2013).

Nonetheless, the majority of the techniques developed for standing wave suppression and correction of focus aberration have been evaluated in simulations, *ex vivo*, and phantoms experiments, except studies with short pulses coded ultrasonic excitation (Choi *et al* 2011, O'Reilly *et al* 2011). However, in the clinical setting, many other parameters interfere with the results of the transcranial ultrasound therapy. As of today, not all mechanisms involved in this form of therapy are fully understood and the aforementioned models unfortunately do not take into account the heterogeneity of soft tissue or the variability of drug uptake and clearance among subjects. Therefore, *in vivo* studies are critical for more complete assessment of therapeutic efficacy and to expand our understanding of the mechanisms involved in the techniques. The use of large phased arrays and short pulse-coded excitation have already been proven valuable in *in vivo* studies. Evidence of the *in vivo* efficacy of the chirp- and random-coded ultrasonic excitation methods in terms of improvement in focusing, suppression of standing waves and effects of multifrequency excitation is, however, currently limited to their imaging capabilities.

In the study reported herein, the capability of the chirp- and random-based coded ultrasonic excitation in improving the targeting of the therapeutic FUS is investigated using an ultrasound-mediated BBB opening protocol in mice. The evaluation of the focusing capability was quantified by the volume of BBB opening and the cavitation dose was evaluated for each technique. The objective was to sweep the frequency linearly or randomly in order to activate differently sized microbubbles and avoid standing wave formation.

2. Methods

The chirp and the periodic selection of random frequency (PSRF) (Furuhata and Saito 2013) coded ultrasonic excitation techniques were first assessed in computational simulations followed by experiments in mice *in vivo*. First, the customized signal generation for both techniques are introduced. Then, the acoustic pressure field generated by the signals are evaluated in simulations with acoustic properties based on μ CT images. Subsequently, sonication was performed for blood brain barrier (BBB) opening, where cavitation was monitored through passive cavitation detection (PCD) in real time. The BBB opening was subsequently imaged by magnetic resonance imaging (MRI). The safety of the methods used was determined through histology of the mouse brains.

2.1. Coded ultrasonic excitation methods

The Chirp and PSRF methods consisted in generating ultrasound-coded transmitting signals that spanned linear or random frequency bandwidths. The signals were composed of sinusoidal waves with the frequency $f(t)$ varying linearly or randomly according to the chosen method. The signals are described by

$$s(t) = K(f(t)) \sin(\phi(t)) \quad (1)$$

where $\phi(t)$ is the time domain function of the phase and $K(f(t))$ is the experimental calibration factor that varies the amplitude of the signals according to the frequency $f(t)$ taking into account the transducer frequency response and the mouse skull attenuation.

2.1.1. Chirp. In the regular linear chirp, the instantaneous frequency varies linearly with time. Here, the signal was customized to allow N full cycles of pulses for each $f(t)$ making $\phi(t)$ constant for a period of time $\frac{N}{f(t)}$. The minimum number of cycles was set to increase the

oscillation of the bubbles and enhance the BBB opening based on a previous study (Choi *et al* 2011). The frequencies shift according to the following series:

$$t_n = N \sum_{i=0}^{n-1} \frac{1}{f_i} \quad (2)$$

where the index n indicates the chosen frequency in the frequency bandwidth $f_n = f_0 + n\Delta f$, where f_0 is the starting frequency and Δf is the frequency step. By integrating the series with an interval f_0 to f_n , the instantaneous frequency $f(t)$ is

$$f_n(t) = f_0 e^{\frac{\Delta f}{N}t} \quad (3)$$

and the chirp signal is given by:

$$s(t) = K(f(t)) \sin\left(2\pi f_0 e^{\frac{\Delta f}{N}t} t\right) \quad (4)$$

2.1.2. PSRF In the random method, the frequencies were randomly sorted using the same frequency bandwidth and interval Δf as the ones used in the chirp method. The frequencies were then varied periodically, the selected frequency was kept constant for the same period $\frac{N}{f(t)}$ adopted in the chirp method, with derivative of the phase angle expressed by (Furuhata and Saito 2013):

$$d\phi_{\text{rand}}(t) = 2\pi f_{\text{rand}}(t) dt \quad (5)$$

2.2. Simulations

2.2.1. μ CT images. The acoustic properties of the mouse head were obtained from μ CT images. One mouse (mass: 24 g, sex: male, C57BL/6, Harlan, Indianapolis, IN, USA) was sacrificed immediately before μ CT scanning and placed in a zip lock bag sprayed with chlorine dioxide. The carcass was secured in a plastic tube and placed in a μ CT scanner (R_mCT2, Rigaku, Tokyo, Japan) where images from a volume of 512 by 512 by 512 pixels and resolution of 80 μ m in the three directions were acquired. The density and sound speed were converted using the Hounsfield units of the coronal slices spanning the caudate putamen (6 mm anterior from Lambda). The conversion of the Hounsfield units to density and sound speed maps was based on experimental data fittings (Schneider *et al* 1996, Mast 2000) using the Hounsfield unit conversion tool provided by the k-Wave Matlab toolbox (Treeby *et al* 2012). The attenuation coefficient for the brain was assumed as 0.6 dB.cm⁻¹ based on soft tissue values (Cobbold 2007). The attenuation coefficient for the skull was set as 29 dB.cm⁻¹ based on the calibration (skull thickness from the μ CT equal to 0.5 mm, ultrasound attenuation in the caudate putamen equal to 15% at 1 MHz). The brain and the skull regions were segmented by thresholding the impedance map obtained by the multiplication of the density and sound speed maps, where $Z_{\text{brain}} = 1.49\text{--}2.00$ MRayls and $Z_{\text{skull}} > 2.00$ MRayls, respectively.

2.2.2. Numerical simulation. The numerical simulations were performed using the k-Wave Matlab toolbox (Treeby *et al* 2012). The toolbox provides the k-space pseudo spectral time domain solution for the coupled first-order acoustic equations for heterogeneous media given by

$$\frac{\partial \mathbf{u}}{\partial t} = -\frac{1}{\rho_0} \nabla p, \quad (6)$$

$$\frac{\partial \rho}{\partial t} = -\rho_0 \nabla \cdot \mathbf{u} - \mathbf{u} \cdot \nabla \rho_0, \quad (7)$$

$$p = c_0^2 (\rho + \mathbf{d} \cdot \nabla \rho_0 - L\rho), \quad (8)$$

where \mathbf{u} is the acoustic particle velocity, p is the acoustic pressure, ρ is the acoustic density, ρ_0 is the equilibrium density, c_0 is the isentropic sound speed, \mathbf{d} is the acoustic particle displacement, and L is the linear integro-differential operator that accounts for acoustic absorption (α) that follows a frequency power law in the form of $\alpha = \alpha_0 \omega^\gamma$. The k-Wave Matlab Toolbox limits the alpha power coefficient γ to a scalar. This limitation does not allow selection of different γ values for each of the different media in the simulation (brain, skull, water). In this simulation, the power law absorption was modeled with the alpha power equal to 1, which is a good assumption for simulating the frequency dependence of soft tissue absorption (Cobbold 2007).

A two-dimensional computational grid was generated covering an area of 80 by 80 mm, with 80 μm of resolution. An ultrasound source with the therapeutic transducer dimensions (focus = 60 mm, aperture = 70 mm, inner hole diameter = 20 mm) was placed on the top of the grid. The source was driven by time-varying pressure signals based on the chirp and PSRF methods (see equation 1) with the calibration factor $K(f(t))$ set constant equal to 1. In addition, a mono frequency sinusoidal time varying pressure source $S(t)$ was simulated to compare with the chirp and PSRF methods.

$$S(t) = A \sin(2\pi ft + \phi_0) \quad (9)$$

where $f = 1.5$ MHz and $A = 1$. The density, sound speed and attenuation maps were loaded in the toolbox workspace with air replacing the void. The ultrasound focal spot was placed on the region of the caudate putamen (anterior/posterior: 6 mm, medial/lateral: 2.2 mm, dorsal/ventral: 3 mm referenced from Lambda). A water cone shaped container was used to couple the source to the mouse skull. The acoustic parameters were varied with the frequency bandwidth ranging from 1.23 to 2.29 MHz, frequency steps (for chirp and random) of 1 kHz and 10 kHz, and number of cycles equal 3. The peak negative pressure (PNP) was recorded in the full 2D computational grid.

Simulations were carried out on a 64-bit workstation (Precision WorkStation T7610, Dell, Austin, TX) with Intel(R) Xeon(R) CPU E5-2630 v2 2.60 GHz processors, 64 GB of RAM and a 6 GB GPU board (Tesla C2075, NVIDIA, Santa Clara, CA, USA).

2.3. Animal preparation

All procedures involving animals were approved and conducted in accordance with the Columbia University Institutional Animal Care and Use Committee. A total of 19 C57BL/6 mice (mass: 20–28 g, sex: male, Harlan, Indianapolis, IN, USA) were used in this study. Two mice were anesthetized with 4% isoflurane and oxygen at 0.8 L.min⁻¹ (SurgiVet, Smiths Medical PM, Inc., Wisconsin, USA), sacrificed with cervical dislocation and used in the calibration. The other 17 mice were anesthetized with 1.0–2.5% isoflurane and oxygen at 0.8 L.min⁻¹ and used in the BBB opening study to be described in the next sections.

2.4. Calibration factor $K(f(t))$

A calibration of the therapeutic transducer (center frequency: 1.94 MHz; -6 dB frequency bandwidth: 1.28–2.31 MHz; diameter: 70 mm; Imasonic SAS, Voray-sur-l'Ognon, France) was conducted with a hydrophone (model HGL-0200, ONDA Corp., Sunnyvale, CA, USA) on 2 freshly excised mouse skulls in a degassed water tank. The skulls were soaked in degassed water for 4 h prior to the calibration. The transducer was attached to a 3D positioning system (Velmex Inc., Bloomfield, NY, USA) and placed above the hydrophone with the focus on the sensitive tip of the hydrophone. The skulls were attached to a secondary 3D positioning system (Velmex Inc., Bloomfield, NY, USA) and carefully placed between the hydrophone and the transducer with the hydrophone sensitive tip positioned in the coordinates corresponding to the caudate putamen (anterior/posterior: 6 mm, medial/lateral: ± 2.2 mm, dorsal/ventral: 3 mm referenced from Lambda). A PC workstation controlled the 3D positioning systems and the digitizer (Gage Applied Technologies Inc., Lachine, QC, Canada) that acquired the ultrasound frequency bandwidth assessed from 0.30 to 3.00 MHz with 0.01 MHz intervals on the left and right caudate putamen of each sample.

2.5. Sonication protocol

Isoflurane was continuously delivered at 1.0% to the mice during the procedure described here (SurgiVet, Smiths Medical PM Inc., Waukesha, WI, USA). The mice had their heads shaved and thereafter immobilized within a stereotaxic frame (David Kopf Instruments, Tujunga, CA, USA). A container filled with degassed water was placed above each mouse with the head coupled to the bottom of the container using coupling gel. The therapeutic transducer (described in section 2.5) and a pulse-echo transducer with their foci overlapping were mounted together with an acrylic cone filled with deionized degassed water. The pulse-echo transducer (center frequency: 10 MHz, focal depth: 60 mm, diameter: 22.4 mm; model U8517133, Olympus NDT, Waltham, MA, USA) was used for targeting and served as a passive cavitation detector for monitoring the cavitation activity in the brain during sonication. The transducer assembly was attached to a 3D positioning system (Velmex Inc., Bloomfield, NY, USA) (figure 1). Both Chirp and PSRF coded excitation signals were generated in Matlab, uploaded to the arbitrary waveform generator (33220A, Agilent Technologies, Palo Alto, CA, USA), driving the therapeutic transducer through a 50 dB power amplifier (325LA, ENI Inc., Rochester, NY, USA).

Immediately prior to sonication of the right caudate putamen, all mice were injected with lipid-shelled, polydisperse microbubbles (table 1) as previously described in Wang *et al* (2015). The left hemisphere of each mouse was left intact as control. The mice were randomly assigned to one of the three groups: Chirp, PSRF, and Regular ($n = 5$ per group). The Chirp group was sonicated using the chirp method with $f_o = 1.5$ MHz, $f_f = 1.9$ MHz, $\Delta f = 10$ kHz, PNP = 0.52 MPa, and $N = 3$ cycles providing a 70.7 μ s pulse length repeating this sequence continuously without interruption for an ON-time of 30 s. The PSRF group was sonicated using the PSRF method with the same parameters. The Regular group was sonicated using a pulsed wave with $f = 1.5$ MHz, 20 ms, 5 Hz of burst rate, 0.52 MPa for 5 min providing a total ON-time of 30 s for all methods used.

2.6. Passive Cavitation Detection

A second arbitrary waveform generator (33220A, Agilent Technologies, Palo Alto, CA, USA) was used to synchronize the therapeutic transducer with the passive cavitation detection (PCD) system at 5 Hz pulse repetition frequency for all types of waveform. The monitoring transducer was connected to a pulser-receiver (NDT-5800, Panametrics, MA, USA) in receiving mode

30 min was allowed before the acquisition of the MRI images. The MRI images (320 by 320 matrix size, spatial resolution of 80 by 80 μm^2 , slice thickness of 400 μm) were generated for all mice with a 2-D FLASH T1-weighted sequence using a 9.4-T microimaging MRI system (DRX400, Bruker BioSpin, Boston, MA, USA). The images were used to determine the BBB opening volume and to assess whether the methods caused any brain damage (i.e. edema). The volume of opening was quantified inside a manually selected ellipsoid covering the sonicated (right) hemisphere of the brain (Samiotaki *et al* 2012). The ellipsoid was set with a major diameter of 5.5 mm, minor diameter of 4.0 mm, and a 0.4 mm height throughout 9 slices. The intensity threshold was determined using the non-sonicated hemisphere as reference and the contrast-enhanced voxels of the vessels and ventricles were excluded. The BBB opening volume was determined counting the total number of voxels with intensity values equal to or above 2.5 standard deviations of the reference.

2.8. Histology

The safety of the applied sonication methods were analyzed with Hematoxylin and Eosin (H&E) stained brain sections. One week after sonication, all mice were transcardially perfused and fixed in 4% paraformaldehyde. Following postfixation processing, the brains were paraffin embedded and then sectioned horizontally at 6 μm thickness in 8 separate levels with 180 μm intervals to cover the caudate putamen. At each level, four sections were acquired and stained with H&E. Bright-field images of the stained sections were acquired using a light microscope (BX61; Olympus, Melville, NY, USA) and were white corrected. Histological evaluation was performed by a trained observer without knowledge of the location and parameters of sonication. The samples were evaluated for red blood cell extravasation into the brain parenchyma as well as cell and tissue loss.

3. Results

The spectral responses of the FUS transducer were obtained from calibration in water and with the hydrophone positioned behind the skull in the caudate putamen region as shown in figure 2(a). The calibration factor $K(f(t))$ was based on the transducer response by taking into account the skull attenuation in targeting the caudate putamen and is provided in figure 2(b). The acoustic pressure was set to be constant within the bandwidth of 1.5 to 1.9 MHz using both chirp (figures 2(c) and (d)) and random-based (figures 2(e) and (f)) methods. The non-variability of the pressure with the frequency was important to avoid a decrease of the bubble-resonance frequency with pressure (Doinikov *et al* 2009). The waveform of the random-based method shows subtle changes in the randomly selected frequencies. The subtle changes in the instantaneous frequency introduce other frequencies in the spectrum that increase some components in the frequency bandwidth.

Figure 3 shows the simulated peak negative pressure fields for the three evaluated methods. The regular sonication presented standing wave formation on the simulations (figure 3(a)). The chirp and random methods were explored by varying the bandwidth, the instantaneous frequency steps $f(t)$ and the number of cycles. For the chirp method, the best parameters found were within the bandwidth of 1.23 to 2.29 MHz (bandwidth of the therapeutic transducer), 10 kHz of frequency steps and 2 cycles (figure 3(d)). In this case, the interference of the waves led to better focusing and lower standing wave formation. In the worst case, (figure 3(c)) higher side lobes and standing waves were observed. Additionally, points of maxima were found outside the focus due to the interference pattern caused by the multiple scattering of

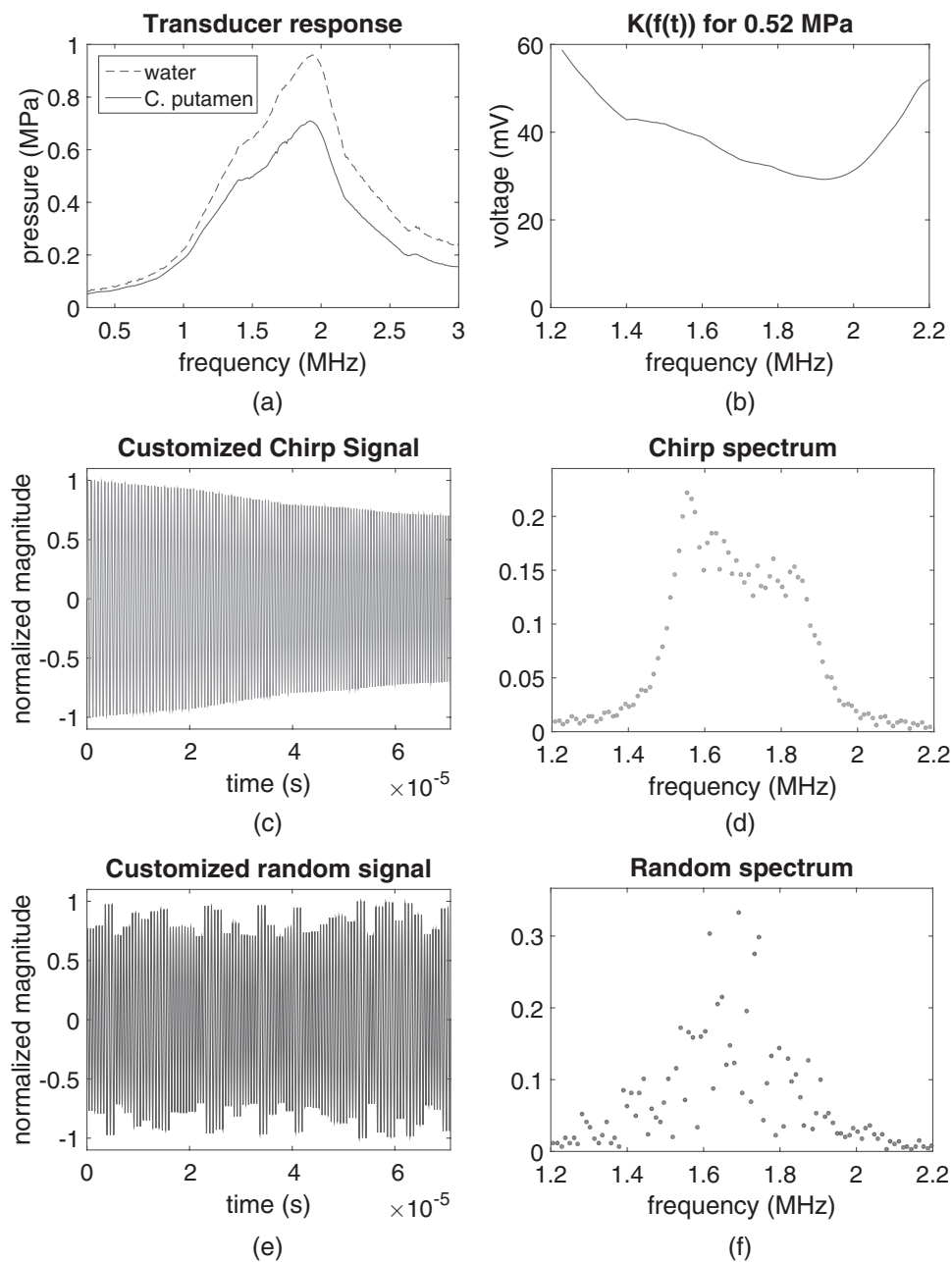


Figure 2. Chirp and PSRF signal characterization. (a) Spectral transducer response (in water) and spectral transducer response with skull attenuation (in caudate putamen region), (b) calibration factor $K(f(t))$ based on the spectral transducer response, (c) customized chirp signal, (d) customized chirp signal spectrum, (e) customized PSRF signal, (f) customized PSRF signal spectrum.

the waves in the brain. The random-based method presented better focusing at 1.23 to 2.29 MHz, 1 kHz of frequency steps and 3 cycles (figure 3(g)). The axial and lateral beam profiles for the three methods are presented in figure 4. Figure 4 shows the beam profiles for the chirp

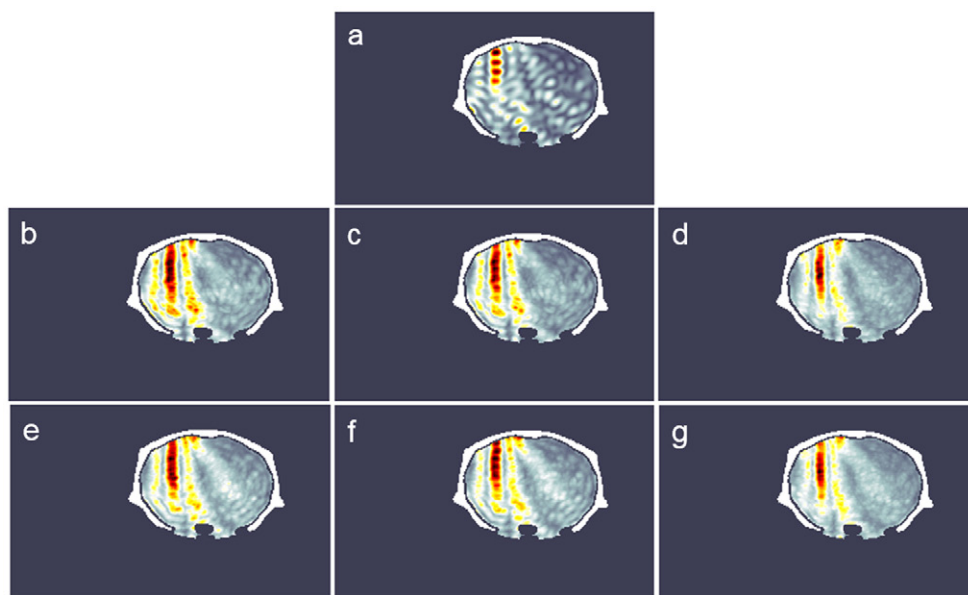


Figure 3. Simulated peak negative pressure fields for: (a) regular sonication (1.5 MHz); (b) chirp: 1.5–1.9 MHz, 10 kHz, 3 cycles; (c) chirp: 1.5–1.9 MHz, 10 kHz, 2 cycles; (d) chirp: 1.23–2.29 MHz, 10 kHz, 3 cycles; (e) random: 1.5–1.9 MHz, 10 kHz, 3 cycles; (f) random: 1.5–1.9 MHz, 1 kHz, 2 cycles; and (g) random: 1.23–2.29 MHz, 1 kHz, 3 cycles.

and random methods, compared to the profile obtained from the regular sonication. The axial profile shows the standing wave formation produced by the regular sonication, which is not observed in the coded methods. The lateral beam profile at the focus shows the side lobes generated by the three techniques. The regular sonication presented higher oscillations on the pressure field with higher peak negative pressure, which is more likely to promote cavitation. The simulation indicates that larger frequency bandwidths provide more effective focusing (figures 3(d) and (g)). However, in the *in vivo* validation, the BBB opening was not consistently achieved using larger frequency bandwidths. Thus, the maximum frequency bandwidth was set from 1.5 to 1.9 MHz (figures 3(b) and (e)) in the experimental results shown here. Further studies are necessary to explore if the frequency bandwidth for obtaining effective BBB opening is limited by the microbubble size.

The PCD detected the frequency components scattered by the microbubbles in the brain vascular system during sonication. The real-time PCD signals for chirp, random, and regular methods are presented in figures 5(a)–(c), respectively. The plots in the middle (figures 5(d)–(f)) show the cavitation level SCD_h calculated for the harmonics of the frequency components for each method. Below each plot are the spectrograms for each method (figures 5(g)–(i)). In the chirp method, the harmonics and ultra-harmonics can be observed in the spectrogram of figure 5(g) where the frequency components increase with time following the linear increase of the instantaneous frequency. In the random method, the spectrogram shows larger harmonic frequency bands characterizing multiple components being scattered over time. The larger frequency band indicates the presence of inertial cavitation and ultimately higher bubble cavitation activity. The regular sonication presented clearly defined harmonic components of the fundamental frequency 1.5 MHz used for this method. Figure 6 shows the ANOVA statistical analysis of the cavitation level (figures 5(d)–(f)). The average cavitation level for the regular

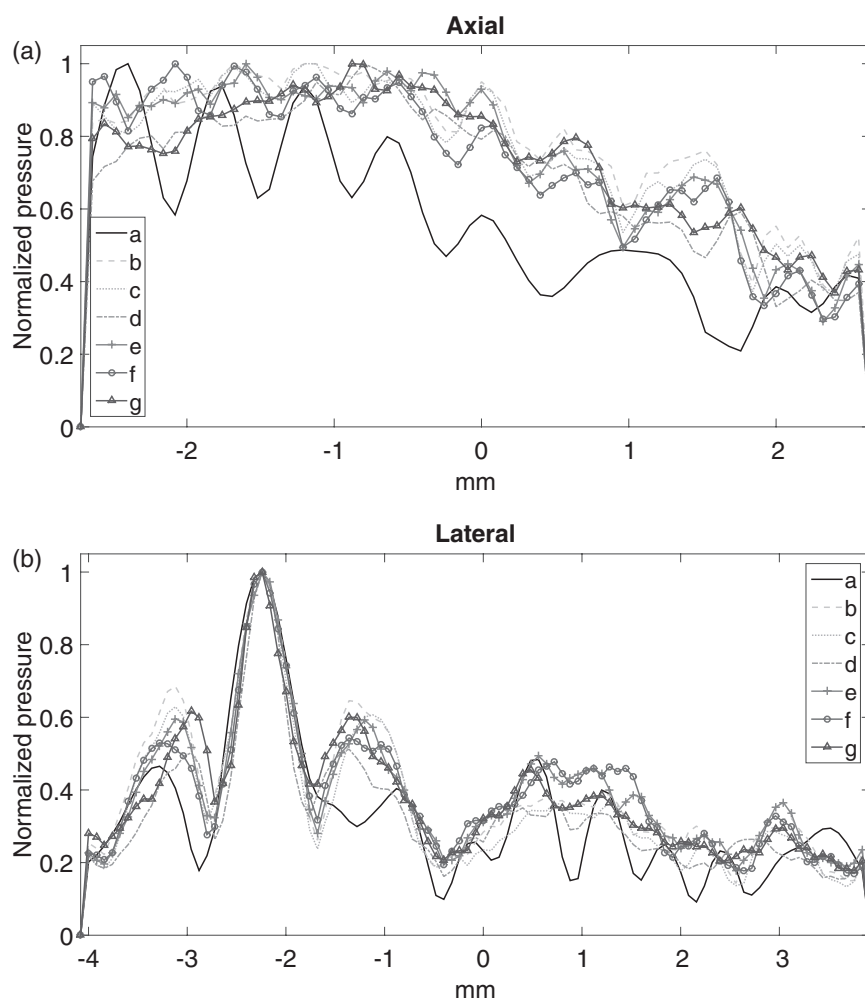


Figure 4. (a) Axial and (b) lateral beam profiles in the focus region obtained from the simulated pressure fields found in figure 3.

sonications was found to be higher than for the coded excitation methods. The mean cavitation levels were 55.40 ± 28.43 V.s, 63.87 ± 29.97 V.s and 356.52 ± 257.15 V.s for the chirp, random and regular sonications, respectively. No significant difference was found between the coded excitation methods.

Figures 7(a)–(f) show T1-FLASH weighted MRI images for the three methods. The brighter regions in the brain show the diffusion of the contrast agent into the brain parenchyma. This region of higher contrast indicates where the ultrasound successfully opened the BBB. The chirp method (figures 7(a) and (d)) and the random-based method (figures 7(b) and (e)) presented smaller openings in comparison to the ones found with the regular sonication method (figures 7(c) and (f)). Figure 7(g) presents the vertical profiles obtained from the coronal MRI images (figures 7(a)–(c)). The first peak is the skull, which was used to align the profiles. The BBB openings observed in the profiles revealed that the ultrasound focus was at 3.60 mm depth in the case of the chirp sonication and at 3.28 mm depth in the random sonication case. Although the coded methods presented more confined BBB opening at the

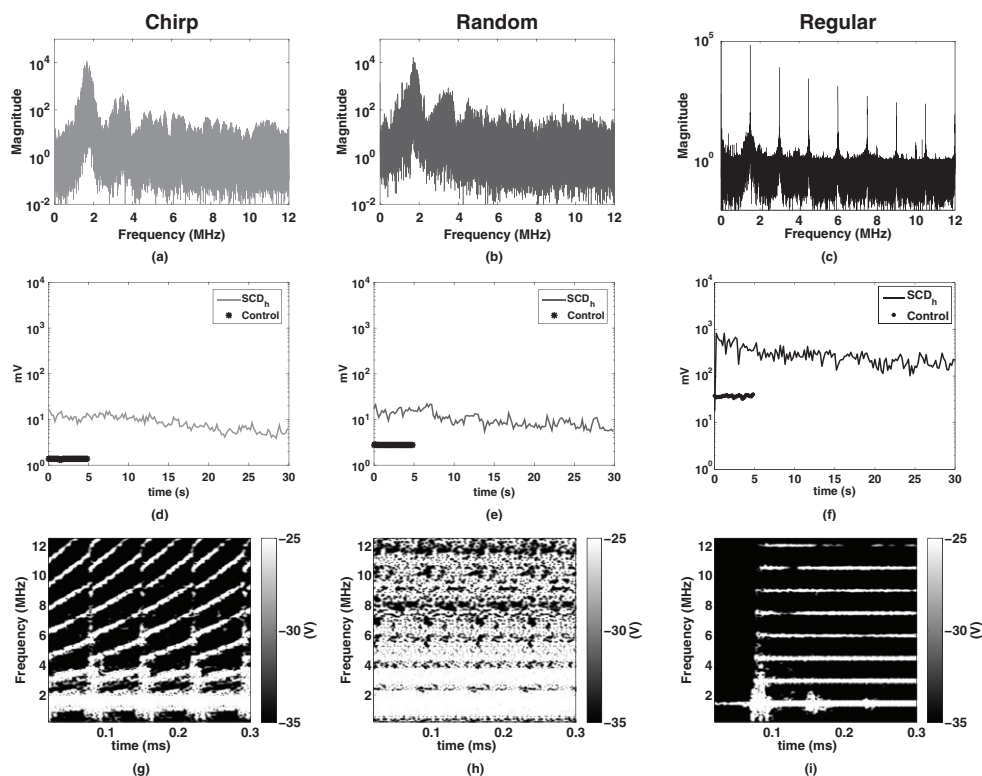


Figure 5. Passive cavitation detection (PCD) monitoring. Frequency spectra obtained from the PCD for (a) chirp, (b) random and (c) regular methods; cavitation levels for each method over the sonication time ((d), (e), and (f), respectively); realtime spectrograms of the PCD signals for each method ((g), (h), and (i), respectively) with the colorbar representing the amplitude of the short-time Fourier transform spectrum.

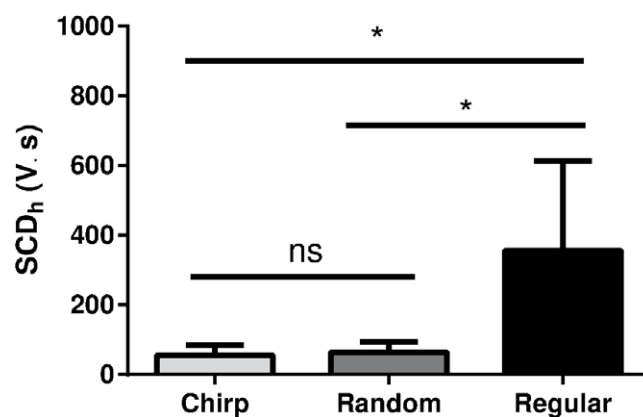


Figure 6. ANOVA statistical analysis of the cavitation levels for each group. No statistically significant difference (ns) was found between the chirp and random groups. Significant differences (*) were found between the regular and chirp groups and regular and random groups.

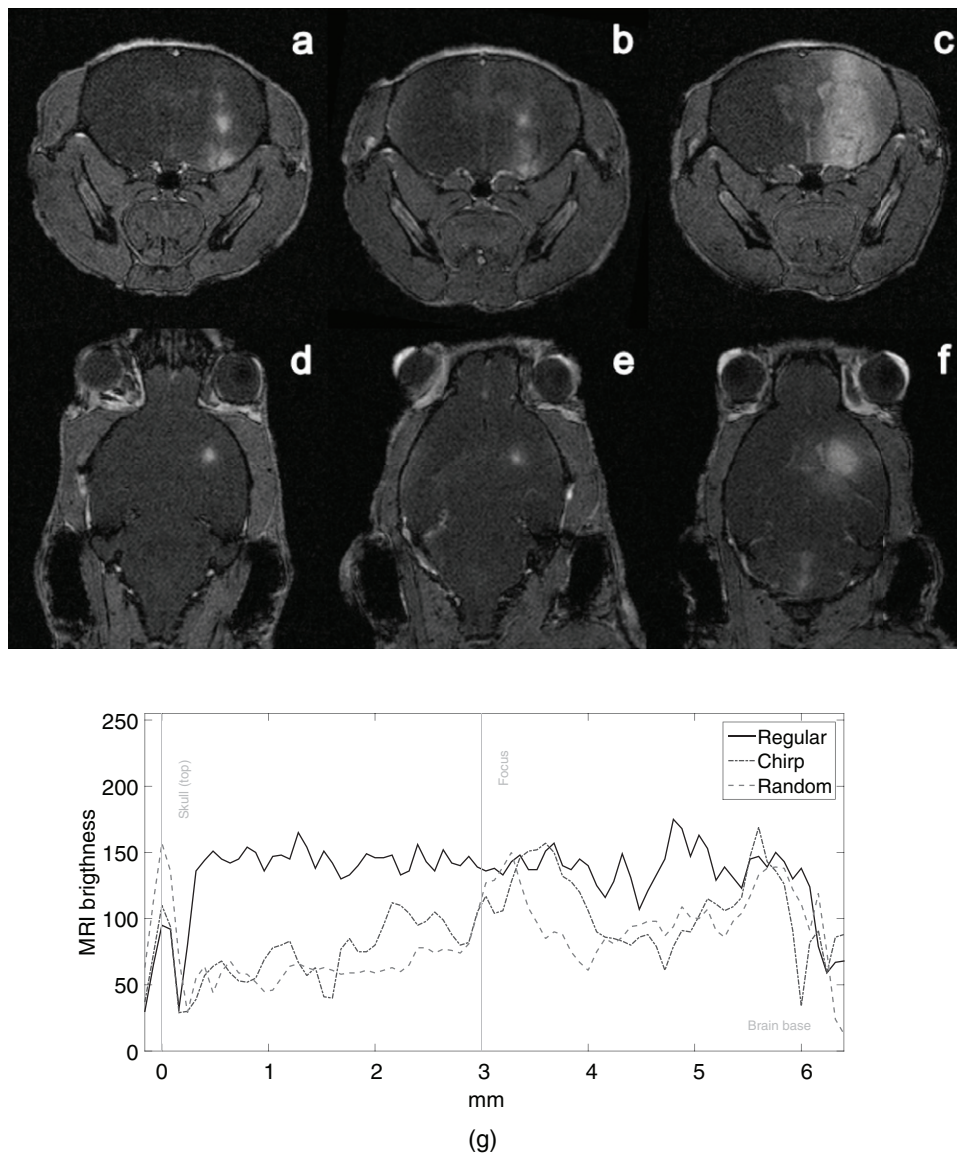


Figure 7. BBB opening evaluation. (a)–(c) Coronal and (d)–(f) transverse T1-FLASH weighted MRI images showing the BBB opening with the use of gadolinium contrast agent for chirp, random and regular sonication methods, respectively and (g) vertical profile extracted from the coronal MRI images (a)–(c).

focus compared to the regular sonication, deeper BBB opening regions were observed close to the skull base at 5.60 mm and 5.76 mm for the chirp and random cases, respectively. The distance from the actual foci to the deeper BBB openings were 2 mm and 2.48 mm for the chirp and random cases, respectively. The opening volumes found for the three groups are presented in figure 8. The mean opening volumes evaluated from the MRI were $9.38 \pm 5.71 \text{ mm}^3$, $8.91 \pm 3.91 \text{ mm}^3$ and $35.47 \pm 5.10 \text{ mm}^3$ for chirp, random and regular sonication, respectively. The regular sonication method presented larger openings. The coded excitation methods did not present significant differences between each other for the opening volumes.

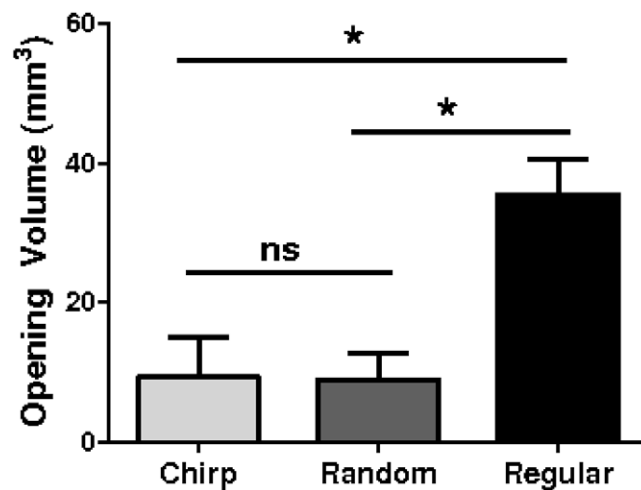


Figure 8. Opening volume quantification for the chirp, random and regular sonication methods. No statistically significant difference (ns) was found between the chirp and random groups. Significant differences (*) were found between the regular and chirp groups and regular and random groups.

Table 1. Microbubbles properties. Measurements^f performed immediately after activation.

	Amount ^a per mL	Mean ^b μm	S.D. ^c μm	C.V. ^d	d10 ^e μm	d50 ^e μm	d90 ^e μm
Sample 1	6.569e9	1.37	1.02	74.5%	0.729	1.07	2.20
Sample 2	6.821e9	1.39	0.991	71.5%	0.729	1.10	2.21

^a Number of particles per mL.

^b Average diameter of microbubbles.

^c Standard deviation of the microbubble diameter distribution.

^d Coefficient of variation in diameter (SD/mean).

^e d10, d50, d90: number of percentile of microbubble diameters.

^f Multisizer 3 Coulter Counter, Beckman Coulter, Fullerton, CA, USA.

No brain damage was detected after performing whole brain histological examination for the animals sonicated with the chirp coded ultrasonic excitation. Four out of five animals from the random-based group presented dark neurons as minor tissue deformation at sonicated sites. Three out of five animals from the regular group died after the second day during the MRI acquisition. The other two mice presented similar minor damage to that found in the random-based animal group.

4. Discussion

Experimental studies have shown a decrease in the microbubble resonance frequency with acoustic pressure (Doinikov *et al* 2009). In this study, a compensation of the pressure amplitude was applied to maintain the acoustic pressure constant for the chirp and random methods. The compensation accounted for the transducer frequency response and attenuation losses through the skull. The frequency spectrum for the PCD chirp shows a linear slope on the $f(t)$

frequency and its harmonics over time. For the PSRF method, the PCD shows bubble activity in bandwidths of 1.5–1.9 MHz and the harmonic bandwidths. The regular sonication shows peaks of activity at the main frequency of 1.5 MHz and its harmonics. These characteristics of the chirp and PSRF methods may allow for the development of bubbles with multiple sizes to improve the efficacy of the sonication. The high cavitation level observed in the regular sonication can be explained due to the use of microbubbles with average size of 1.4 μm , which have a resonance frequency of 1.5 MHz.

The coded excitation methods were continuously driven to facilitate the standing wave formation caused by multiple scattering of the wave inside the brain. The coded methods were capable of avoiding the standing wave formation as predicted by the simulations. However, the coded excitation methods were not capable of avoiding BBB openings close to the skull base, which were observed in all methods. The standing wave peaks were expected to have distances between 0.4 mm and 0.5 mm that correspond to half wavelengths of the frequency bandwidth limits 1.9 MHz and 1.5 MHz, respectively (assuming $c = 1540 \text{ m s}^{-1}$). Multiple scattering of the waves inside the skull may have caused aberration of the focus. The lower cavitation levels detected for the coded excitation methods indicate lower microbubble activity, which was confirmed with the more confined openings detected by the MRI images. These results corroborate with other studies that have demonstrated the cavitation reduction using random methods (Chapelon *et al* 1996, Furuhashi and Saito 2013). Hence, the coded methods were capable of enhancing targeting for BBB opening.

The replenishment of the microbubbles allowed by the pulsed excitation used in the regular sonication generated larger openings. The larger openings for this group can also be explained by the narrower distribution of the microbubble size, which in this case caused the single frequency to engage a larger number of microbubbles at their corresponding resonance frequencies.

The variation of the BBB opening volume indicates possible differences arising from non-uniform tissue properties and animal dependency. These physiological discrepancies can attribute to the variation of microbubble replenishment through circulation and the probability of interaction of the bubbles with the BBB.

The coded ultrasonic methods were proven capable of improving the targeting capabilities in BBB opening. However, application of the in range equation through the skull varied among animals affecting thus the focus positioning procedure which led to, albeit small, differences between the actual and the expected focus position, 0.60 mm and 0.28 mm for chirp and random, respectively. Using a larger bandwidth was found to achieve better focusing and reduce standing wave formation for the coded methods. It is important to note that the choice of frequency bandwidth needs to take into account the frequency response of the transducer, the skull attenuation and the microbubble optimum frequency range. The higher focusing capability found here improves the targeting precision of the method for specific regions of the brain to be treated with drugs and other pharmacological substances. The coded methods can be easily implemented in different setups. The use of these methods together with large phased arrays may improve the focusing and reduce SW formation. Therefore, other techniques could also benefit by this coded excitation method, e.g. sonothrombolysis for reduction of hemorrhage. The higher targeting performance is an important advantage especially for HIFU which uses higher pressure levels and needs to be very precise to ablate the prescribed region and avoid damage to the healthy tissue.

The microbubble size restricts the frequency bandwidth that can be used in the coded methods. Therefore, further studies are necessary to explore different microbubble size distributions and shell properties (Wu *et al* 2015) and their corresponding effective resonance frequencies. The microbubble response could also be taken into account for determining the

calibration factor $K(f(t))$. Incorporating this aspect would increase the efficacy of the method by improving the use of all available bubble sizes.

5. Conclusion

In summary, evidence on the associated improvements in targeting through the skull using coded ultrasonic excitation based on chirp and random modulations were quantified *in vivo*. We assessed customized ultrasound transmit sequences in which frequencies were linearly or randomly swept. These sequences were shown to be capable of inducing a more confined BBB opening volume. This methodology could prove equally beneficial in other transcranial therapeutic ultrasound applications to improve targeting and prevent collateral damage. Furthermore, these methods provide the possibility of exploring the effects of multi-frequency excitation as a tool to expand our understanding of the mechanisms involved in transcranial therapeutic ultrasound and its effects on the brain tissue.

Acknowledgments

This study was supported in part by NIH (R01EB009041 and R01AG038961) and FAPESP (2011/10809-6 and 2013/08116-8). We thank Hong Chen, PhD and Tenysson W Lemos, PhD for their important input and technical support.

References

- Alexandrov A V 2009 Ultrasound enhancement of fibrinolysis *Stroke* **40** 107–10
- Alonso A, Reinz E, Leuchs B, Kleinschmidt J, Fatar M, Geers B, Lentacker I, Hennerici M G, de Smedt S C and Meairs S 2013 Focal delivery of AAV2/1-transgenes into the rat brain by localized ultrasound-induced BBB opening *Mol. Ther.: Nucleic Acids* **2** e73
- Baseri B, Choi J J, Deffieux T, Samiotaki G, Tung Y S, Olumolade O, Small S A, Morrison B and Konofagou E E 2012 Activation of signaling pathways following localized delivery of systemically administered neurotrophic factors across the blood-brain barrier using focused ultrasound and microbubbles *Phys. Med. Biol.* **57** N65–81
- Burgess A, Ayala-Grosso C A, Ganguly M, Jordao J F, Aubert I and Hynynen K 2011 Targeted delivery of neural stem cells to the brain using MRI-guided focused ultrasound to disrupt the blood-brain barrier *PLOS One* **6** e27877
- Chang J W, Min B K, Kim B S, Chang W S and Lee Y H 2015 Neurophysiologic correlates of sonication treatment in patients with essential tremor *Ultrasound Med. Biol.* **41** 124–31
- Chapelon J, Dupenloup F, Cohen H and Lenz P 1996 Reduction of cavitation using pseudorandom signals *IEEE Trans. Ultrason. Ferroelectr. Freq. Control* **43** 623–5
- Choi J J, Pernot M, Small S A and Konofagou E E 2007 Noninvasive, transcranial and localized opening of the blood-brain barrier using focused ultrasound in mice *Ultrasound Med. Biol.* **33** 95–104
- Choi J, Selert K, Vlachos F, Wong A and Konofagou E E 2011 Noninvasive and localized neuronal delivery using short ultrasonic pulses and microbubbles *Proc. Natl Acad. Sci. USA* **108** 16539–44
- Cobbold R S C 2007 *Foundations of Biomedical Ultrasound* (Oxford: Oxford University Press)
- Coluccia D, Fandino J, Schwyzer L, OGorman R, Remonda L, Anon J, Martin E and Werner B 2014 First noninvasive thermal ablation of a brain tumor with mr-guided focused ultrasound *J. Therapeutic Ultrasound* **2** 1–7
- Daffertshofer M, Gass A, Ringleb P, Sitzler M, Sliwka U, Els T, Sedlacek O, Koroshetz W J and Hennerici M G 2005 Transcranial low-frequency ultrasound-mediated thrombolysis in brain ischemia—increased risk of hemorrhage with combined ultrasound and tissue plasminogen activator—results of a phase II clinical trial *Stroke* **36** 1441–6
- Deffieux T and Konofagou E E 2010 Numerical study of a simple transcranial focused ultrasound system applied to blood-brain barrier opening *IEEE Trans. Ultrason. Ferroelectr. Freq. Control* **57** 2637–53

- Deffieux T, Younan Y, Wattiez N, Tanter M, Pouget P and Aubry J F 2013 Low-intensity focused ultrasound modulates monkey visuomotor behavior *Current Biol.* **23** 2430–3
- Doinikov A A, Haac J F and Dayton P A 2009 Resonance frequencies of lipid-shelled microbubbles in the regime of nonlinear oscillations *Ultrasonics* **49** 263–8
- Elias W et al 2013 A pilot study of focused ultrasound thalamotomy for essential tremor *N. Engl. J. Med.* **369** 640–8
- Furuhata H and Saito O 2013 Comparative study of standing wave reduction methods using random modulation for transcranial ultrasonication *Ultrasound Med. Biol.* **39** 1440–50
- Hynynen K and Jolesz F A 1998 Demonstration of potential noninvasive ultrasound brain therapy through an intact skull *Ultrasound Med. Biol.* **24** 275–83
- Hynynen K, McDannold N, Clement G, Jolesz F A, Zadicario E, Killiany R, Moore T and Rosen D 2006 Pre-clinical testing of a phased array ultrasound system for MRI-guided noninvasive surgery of the brain: a primate study *Eur. J. Radiol.* **59** 149–56
- Hynynen K, McDannold N, Vykhodtseva N and Jolesz F A 2001 Noninvasive MR imaging-guided focal opening of the blood-brain barrier in rabbits *Radiology* **220** 640–6
- Kamimura H A S, Pavan T Z, Carneiro A A O, Pinto P T C and Neto O M P 2013 Nonlinear mixing of two ultrasonic beams for transcranial sonothrombolysis *IEEE Int. Ultrasonics Symp.* pp 2103–5
- King R L, Brown J R, Newsome W T and Pauly K B 2013 Effective parameters for ultrasound-induced in vivo neurostimulation *Ultrasound Med. Biol.* **39** 312–31
- Kinoshita M, McDannold N, Jolesz F A and Hynynen K 2006 Noninvasive localized delivery of herceptin to the mouse brain by MRI-guided focused ultrasound-induced blood-brain barrier disruption *Proc. Natl Acad. Sci. USA* **103** 11719–23
- Marquet F, Boch A L, Pernot M, Montaldo G, Seilhean D, Fink M, Tanter M and Aubry J F 2013 Non-invasive ultrasonic surgery of the brain in non-human primates *J. Acoust. Soc. Am.* **134** 1632–9
- Martin E, Jeanmonod D, Morel A, Zadicario E and Werner B 2009 High-intensity focused ultrasound for noninvasive functional neurosurgery *Ann. Neurology* **66** 858–61
- Mast T D 2000 Empirical relationships between acoustic parameters in human soft tissues *Acoust. Res. Lett.* **1** 37–42
- Meairs S, Alonso A and Hennerici M G 2012 Progress in sonothrombolysis for the treatment of stroke *Stroke* **43** 1706–10
- Mitri F G, Greenleaf J F and Fatemi M 2005 Chirp imaging vibro-acoustography for removing the ultrasound standing wave artifact *IEEE Trans. Med. Imaging* **24** 1249–55
- Molina C A et al 2009 Transcranial ultrasound in clinical sonothrombolysis (TUCSON) trial *Ann. Neurology* **66** 28–38
- O'Donnell M 1992 Coded excitation system for improving the penetration of real-time phased-array imaging systems *IEEE Trans. Ultrason. Ferroelectr. Freq. Control* **39** 341–51
- O'Reilly M, Waspe A, Ganguly M and Hynynen K 2011 Focused-ultrasound disruption of the blood-brain barrier using closely-timed short pulses: influence of sonication parameters and injection rate *Ultrasound Med. Biol.* **37** 587–94
- Pajak D and Hynynen K 2013 The application of sparse arrays in high frequency transcranial focused ultrasound therapy: a simulation study *Med. Phys.* **40** 122901
- Pedersen H P, Misaridis T X and Jensen J A 2003 Clinical evaluation of chirp-coded excitation in medical ultrasound *Ultrasound Med. Biol.* **29** 895–905
- Raymond S B, Treat L H, Dewey J D, McDannold N J, Hynynen K and Bacskai B J 2008 Ultrasound enhanced delivery of molecular imaging and therapeutic agents in Alzheimer's disease mouse models *PLOS One* **3** e2175
- Samiotaki G, Vlachos F, Tung Y S and Konofagou E E 2012 A quantitative pressure and microbubble-size dependence study of focused ultrasound-induced blood-brain barrier opening reversibility in vivo using MRI *Magn. Reson. Med.* **67** 769–77
- Schneider U, Pedroni E and Lomax A 1996 The calibration of CT hounsfield units for radiotherapy treatment planning *Phys. Med. Biol.* **41** 111–24
- Tang S C and Clement G T 2010 Standing-wave suppression for transcranial ultrasound by random modulation *IEEE Trans. Biomed. Eng.* **57** 203–5
- Treeby B E, Jaros J, Rendell A P and Cox B T 2012 Modeling nonlinear ultrasound propagation in heterogeneous media with power law absorption using a k-space pseudospectral method *J. Acoust. Soc. Am.* **131** 4324–36
- Tsivgoulis G, Eggers J, Ribo M, Perren F, Saqqur M, Rubiera M, Sergentanis T N, Vadikolias K, Larrue V and Molina C A 2010 Safety and efficacy of ultrasound-enhanced thrombolysis a comprehensive review and meta-analysis of randomized and nonrandomized studies *Stroke* **41** 280–7

- Tyler W J, Tufail Y, Finsterwald M, Tauchmann M L, Olson E J and Majestic C 2008 Remote excitation of neuronal circuits using low-intensity, low-frequency ultrasound *PLOS One* **3** e3511
- Wang S, Olumolade O O, Sun T, Samiotaki G and Konofagou E E 2015 Noninvasive, neuron-specific gene therapy can be facilitated by focused ultrasound and recombinant adeno-associated virus *Genetics Ther.* **22** 104–10
- Wu S Y, Chen C, Tung Y, Olumolade O and Konofagou E 2015 Effects of the microbubble shell physicochemical properties on ultrasound-mediated drug delivery to the brain *J. Control. Release* **212** 30–40
- Wu S Y, Tung Y S, Marquet F, Downs M E, Sanchez C S, Chen C C, Ferrera V and Konofagou E E 2014 Transcranial cavitation detection in primates during blood-brain barrier opening: a performance assessment study *IEEE Trans. Ultrason. Ferroelectr. Freq. Control* **61** 966–78